

USING GENETIC MOUSE MODELS TO STUDY THE BIOLOGY AND PATHOLOGY OF AUTOPHAGY IN THE CENTRAL NERVOUS SYSTEM

Zhenyu Yue,^{*} Gay R. Holstein,^{*} Brian T. Chait,[†]
and Qing Jun Wang^{*,†}

Contents

| | |
|---|-----|
| 1. Introduction | 160 |
| 1.1. Morphological evidence of autophagy in human neurological diseases | 160 |
| 1.2. Basal level of autophagy in the CNS | 161 |
| 1.3. Neuropathology associated with the accumulation of autophagosomes: Impaired versus induced autophagy | 162 |
| 1.4. Essential role of autophagy in axons: Maintenance of homeostasis at the axon terminals | 163 |
| 2. Methods | 164 |
| 2.1. Transgenic reporter mice GFP-LC3 | 164 |
| 2.2. Genotyping GFP-LC3 mice | 164 |
| 2.3. Maintaining GFP-LC3 mice | 165 |
| 2.4. Breeding GFP-LC3 mice to other mouse models | 166 |
| 3. Analysis of GFP-LC3 Expression and Subcellular Localization in the CNS | 167 |
| 4. Analysis of p62/SQSTM1 and Ubiquitinated Protein Inclusions in the CNS | 171 |
| 4.1. Immunohistochemistry staining of p62/SQSTM1 | 171 |
| 5. Transmission Electron Microscopy (TEM) Analysis of Autophagosomes | 173 |
| 5.1. Tissue fixation and processing for ultrastructural studies | 173 |

^{*} Departments of Neurology and Neuroscience, Mount Sinai School of Medicine, New York, New York, USA

[†] Laboratory of Mass Spectrometry and Gaseous Ion Chemistry, Rockefeller University, New York, New York, USA

| | |
|--|-----|
| 5.2. Tissue fixation and processing for pre-embedding immuno-electron microscopy | 174 |
| 5.3. Tissue fixation and processing for post-embedding immunogold TEM localization | 175 |
| 5.4. TEM identification of double-membraned vacuoles | 176 |
| 5.5. Quantification of double-membraned vacuoles | 177 |
| 6. Conclusion | 177 |
| Acknowledgments | 178 |
| References | 178 |

Abstract

Autophagy is a cellular self-eating process that plays an important role in neuroprotection as well as neuronal injury and death. The detailed pathway of autophagy in these two opposing functions remains to be elucidated. Neurons are highly specialized, postmitotic cells that are typically composed of a soma (cell body), a dendritic tree, and an axon. Here, we describe methods for studying autophagy in the central nervous system (CNS). The first involves the use of recently developed transgenic mice expressing the fluorescent autophagosome marker, GFP-LC3. Although CNS neurons show little evidence for the presence of GFP-LC3-containing puncta under normal conditions, under pathological conditions such neurons exhibit many GFP-LC3 puncta. The onset and density of GFP-LC3 puncta have been found to vary significantly in the sub-compartments of the affected neurons. These studies suggest that autophagy is distinctly regulated in CNS neurons and that neuronal autophagy can be highly compartmentalized. While transgenic mice expressing GFP-LC3 are a valuable tool for assessing autophagic activity in the CNS, caution needs to be taken when interpreting results solely based on the presence of GFP-LC3 puncta. Therefore, traditional ultrastructural analysis using electron microscopy remains an important tool for studying autophagosomes *in vivo*. Additional reporters of autophagy are constantly being sought. For example, recently a selective substrate of autophagy p62/SQSTM1 has been shown to be specifically regulated by autophagic activity. Therefore, p62/SQSTM1 protein levels can be used as an additional reporter for autophagic activity.

1. INTRODUCTION

1.1. Morphological evidence of autophagy in human neurological diseases

There are several excellent reviews covering the topic of autophagy in neurons and human neurological diseases (Chu, 2006; Martinez-Vicente *et al.*, 2005; Nixon, 2006; Rubinsztein *et al.*, 2005). Autophagy was first noticed in injured neurons following axotomy or excitotoxicity (Dixon, 1967;

Matthews and Raisman, 1972). These early studies show that autophagy is frequently associated with axonal stumps (swellings) at lesions, or structures highly related to axon swellings. Recently, autophagic activity (as evidenced by the accumulation of autophagosomes) was found in dysfunctional or degenerating neurons of human brains suffering from neurological diseases, such as Alzheimer's disease (AD), Parkinson's disease (PD), Huntington's disease (HD), and Creutzfeldt-Jakob disease (Anglade *et al.*, 1997; Cataldo *et al.*, 1996; Roizin *et al.*, 1974; Sikorska *et al.*, 2004). For example, in neocortical biopsies from AD brain, large numbers of autophagosomes are observed in perikarya and dystrophic neuritic processes of affected neurons (Nixon *et al.*, 2005). Consistent with the involvement of autophagy in neurodegenerative conditions, genetic disruption of cathepsin D and double deletion for cathepsin B and L in mice induce formation of autophagosomes/autolysosomes in many types of neurons, a scenario closely resembling Batten disease/lysosomal storage disorders (LSDs) (Koike *et al.*, 2005). Neuronal death associated with Niemann-Pick type C disease, a LSD, was recently linked to autophagic action (Ko *et al.*, 2005; Pacheco *et al.*, 2007). Hence, historically autophagy is thought to be expressed excessively in many neurological disorders and suspected to be destructive under those conditions. However, the molecular mechanism whereby autophagy contributes to the neuropathogenesis remains to be shown. For example, it is unclear whether hyperactive or impaired autophagy is involved in the neuropathogenesis. Although many neurological diseases are associated with the accumulation of autophagosomes/autolysosomes, the result can be explained by at least two distinct possibilities: up-regulation of autophagosome biogenesis and blockade in autophagosome maturation/disposal of autophagosomes. More important, a causative role of autophagy in neuropathogenesis remains to be established. To address these questions, it is imperative to develop reliable autophagy assays in neurons by which we can assess how autophagy participates in the progression of neurological disease.

1.2. Basal level of autophagy in the CNS

Autophagy is a key lysosomal pathway, which is responsible for the degradation of long-lived proteins and the turnover of cellular organelles in virtually all cell types. The autophagic process is characterized by the formation, maturation and degradation/recycling of double-membrane bound vacuoles called autophagosomes. Autophagy is generally viewed as a stress-induced process for cells to cope with nutrient and energy crises and to promote cell survival, and until recently the role of autophagy under normal conditions remained unrecognized and hence was considered trivial or was ignored. GFP-LC3 transgenic mice exhibit GFP-containing puncta (an indication of autophagosomes) in many different tissues even under normal conditions, revealing the presence of constitutive (basal) autophagy

(Mizushima *et al.*, 2004). However, the CNS appears to be an exception; GFP-LC3 is observed to be mostly diffuse with no GFP-LC3 puncta even in fasting mice (Mizushima *et al.*, 2004). Indeed, double-membraned autophagosomes are rarely seen in healthy neurons (Nixon *et al.*, 2005). While this evidence seems to suggest that autophagy remains under tight control in CNS neurons (by maintaining the process at a very low level), the most recent studies in knock-out mice with targeted deletion of *Atg5* or *Atg7* unequivocally demonstrate the importance of a basal level of autophagy in CNS neurons (Hara *et al.*, 2006; Komatsu *et al.*, 2006). Our study in mutant mice with Purkinje cell-specific deletion of *Atg7* further reveals that autophagy is essential for prevention of axonal dystrophy and degeneration (Komatsu *et al.*, 2007b). Taken together, these studies clearly establish that autophagy is constitutively active in CNS neurons and plays an important role in the maintenance of protein and membrane homeostasis in CNS neurons. However, it seems paradoxical that autophagy is constitutively active despite the absence of GFP-LC3 puncta, suggesting that the lack of GFP-LC3 puncta does not necessarily reflect the absence of autophagic activity in CNS neurons. This observation raises an important question as to how autophagic activity can be correctly measured at the endogenous level, especially under normal conditions when GFP-LC3 puncta are rarely observed. Moreover, the degree of vulnerability of neurons to dystrophy and degeneration upon the loss of autophagy varies significantly among different neuronal types, suggesting a cell type-specific cellular response to autophagy deficiency (Hara *et al.*, 2006; Komatsu *et al.*, 2006). Therefore, it is also critical to investigate cell type-specific autophagy in neuron populations that are specifically affected in certain human diseases.

1.3. Neuropathology associated with the accumulation of autophagosomes: Impaired versus induced autophagy

Increasing evidence indicates that an elevated number of GFP-LC3 puncta (or alternatively the level of the lipidated form of LC3 (LC3-II)) do not always correlate with up-regulated autophagic activity. As discussed in other chapters, in addition to mechanisms that stimulate the formation of autophagosomes, many events that block autophagic degradation may give rise to an increase in the steady-state number of autophagosomes and elevated levels of LC3-II (see also the chapter by Kimura *et al.*, in volume 452). A block of autophagy may occur at many steps including autophagosome maturation, autophagosome-lysosome fusion or lysosomal degradation. For example, in genetic animal models for juvenile neuronal ceroid lipofuscinosis (Cao *et al.*, 2006) and LSDs (Settembre *et al.*, 2008) where the neuropathologies are associated with the accumulation of autophagosomes, autophagy deficiency in neurons is likely due to impaired autophagosome

maturation or lysosomal fusion (Settembre *et al.*, 2008). Two recent studies show that mutations of the ESCRT-III subunit CHMP2B, which are associated with frontotemporal dementia and amyotrophic lateral sclerosis (ALS), can lead to a block of autophagy and the subsequent accumulation of autophagosomes, presumably by interfering with the fusion between multi-vesicular bodies/late endosomes and autophagosomes (Filimonenko *et al.*, 2007; Lee *et al.*, 2007). The preceding evidence argues strongly that assaying only the number of autophagosomes (based on GFP-LC3-labeled puncta) cannot allow the correct interpretation of autophagic activity under neuropathological conditions.

Moreover, although autophagy is traditionally thought to be a mechanism for nonselective degradation, emerging evidence has pointed to a role of selective degradation for autophagy under certain circumstances. For example, recent studies show that autophagy regulates static levels of p62/SQSTM1 protein, which binds to both ubiquitin and LC3 and plays an important role in the formation of ubiquitinated protein inclusions (Bjørkøy *et al.*, 2005; Komatsu *et al.*, 2007a). We find that steady-state levels of p62/SQSTM1 protein are inversely correlated with autophagic activity (Wang *et al.*, 2006) (see also the chapter by Bjørkøy *et al.*, in this volume). Using p62/SQSTM1 as a readout, we have shown that the excitotoxic *Lurcher* mutation induces, rather than blocks, autophagy because *Lurcher* Purkinje cells accumulate a large number of autophagosomes without an increase in p62/SQSTM1 protein levels (Wang *et al.*, 2006). In addition, a recent study shows that hypoxia-ischemic injury in neonatal mouse brain causes extensive neuronal death accompanied by increased autophagosome formation. This increased number of autophagosomes is likely associated with autophagy activation, because a block of autophagy largely prevents neurodegeneration induced by hypoxia-ischemia (Koike *et al.*, 2008).

These data show that tight control of autophagy is necessary for maintaining the health of CNS neurons; deregulation of neuronal autophagy (either too much or too little) is deleterious. One technical challenge facing us today is the development of robust *in vivo* assays for autophagy, which are essential for the understanding of the exact role of autophagy in neuropathogenesis.

1.4. Essential role of autophagy in axons: Maintenance of homeostasis at the axon terminals

To elucidate the physiological role of neuronal autophagy, we generated mutant mice containing a neural cell type-specific deletion of *Atg7*, an essential gene for autophagy. Characterization of these mutant mice reveals a cell-autonomous function of autophagy in cerebellar Purkinje cells. Our results demonstrate the indispensability of autophagy in the maintenance of axonal homeostasis and the prevention of axonal dystrophy and

degeneration under normal conditions (Komatsu *et al.*, 2007b). These results raise interesting questions as to how autophagy proceeds in the axon, which is a highly differentiated neuronal compartment that performs many functions independent of the soma. Since autophagy induction that occurs rapidly in *Lurcher* Purkinje cell axons involves the formation of a large number of autophagosomes in the dystrophic axon terminals (Wang *et al.*, 2006), we hypothesize that autophagosomes may be synthesized locally in axon terminals (especially under pathological conditions) and may undergo axonal transport to the soma where lysosomes are normally present for degradation. To test this hypothesis, we have attempted to set up an *in vitro* system to investigate autophagosome biogenesis and transport in the axons by using a dissociated neuronal culture expressing GFP-LC3, and by live imaging of the behavior of GFP-LC3 puncta (Yue, 2007).

2. METHODS

2.1. Transgenic reporter mice GFP-LC3

GFP-LC3 mice (in the background of C57BL/6j) were originally generated by Mizushima *et al.* (2004) and are now distributed by the RIKEN Bio-Resource Center in Japan (<http://www.brc.riken.jp/lab/animal/en/dist.shtml>). GFP-LC3 mice have now been widely used for monitoring autophagosomes in tissues including the CNS, and provide researchers with an important tool to study autophagic activity *in vivo*.

2.2. Genotyping GFP-LC3 mice

1. Clip the mouse tail (0.3–0.5 cm) and incubate it in a microcentrifuge tube containing 500 μl of tail DNA extraction buffer (100 mM Tris-HCl, pH 8.0, 200 mM NaCl, 5 mM EDTA, 0.2% SDS) supplemented with 10 μl of proteinase K (10 $\mu\text{g}/\mu\text{l}$ stock) at 55 °C overnight. Note that proteinase K should be made fresh or kept frozen to avoid self-digestion.
2. Mix the digested sample by inverting the tube 5 times (avoid vortexing), then centrifuge at 13,000g for 2 min. Transfer the supernatant fraction to a new tube and discard the pellet fraction.
3. Precipitate the DNA by mixing the supernatant fraction with an equal volume of isopropanol, and centrifuge at 13,000g for 1 min.
4. Aspirate off the supernatant Wash the DNA pellet with 1 ml of 70% ethanol.
5. Discard the ethanol and air-dry the DNA pellet for 10 min at room temperature.
6. Resuspend the DNA pellet with 200 μl of TE buffer (10 mM Tris-HCl, pH 7.5, 1 mM EDTA) and incubate the sample at 42 °C for 1 h or until

the DNA pellet is fully dissolved. The DNA concentration is measured and adjusted to 100 ng/ μ l in TE buffer. The DNA prepared using this method can be used for the polymerase chain reaction (PCR) and Southern blot analysis.

7. Take 1 μ l of DNA as the template for the PCR. The following primers are designed to amplify a fragment of GFP. The forward primer sequence is 5'-CCT ACG GCG TGC AGT GCT TCA GC-3'. The reverse primer sequence is 5'-CGG CGA GCT GCA CGC TGC GTC CTC-3'. And the PCR is performed using the QIAGEN Tag DNA Polymerase Kit. Each reaction mixture (20 μ l total volume) contains 10 μ l of double-distilled H₂O, 4 μ l of Q solution, 2 μ l of 10x buffer, 0.8 μ l of 25 mM MgCl₂, 1.6 μ l of 2.5 mM dNTP mixture, 0.2 μ l of 10 μ M forward primer, 0.2 μ l of 10 μ M reverse primer, 0.2 μ l of Tag DNA Polymerase, and 1 μ l of DNA template DNA. The PCR conditions are as follows:

Step 1. 94 °C for 3 min

Step 2. 94 °C for 30 s

Step 3. 60 °C for 30 s

Step 4. 72 °C for 90 s

Step 5. Repeat steps 2–4, 32 times

Step 6. 72 °C for 5 min

8. Analyze the PCR-amplified DNA product on a 1% agarose gel.
Alternative: We have successfully genotyped GFP-LC3 in the neonatal mice (< P10) by visualizing directly GFP fluorescence of the clipped tails. Briefly, place the freshly clipped tail on a glass slide and observe green fluorescence under an inverted fluorescence microscope. The GFP-LC3 transgenic tail normally contains intense and uniform fluorescence and can be easily distinguished from that of a wild-type littermate. Note that this simple typing method is highly reliable with neonates, but not with adult mice.

2.3. Maintaining GFP-LC3 mice

To avoid uncertain effects of transgene insertion in homozygous mice, we recommend that GFP-LC3 mice are maintained as hemizygous (one allele of the transgene). Thus, only one breeder (either male or female) from each breeding pair should contain the GFP-LC3 transgene for genetic crossing, whereas the other breeder should be wild-type (C57BL/6j). However, under some circumstance, GFP-LC3 breeders can be maintained as homozygous to increase the breeding efficiency for having a large number of GFP-LC3-positive offspring in one generation. Recently, the integration site of the GFP-LC3 transgene in the widely used GFP-LC3 line (#53) was

identified, allowing the design of specific primers and employing PCR to identify the homozygous GFP-LC3 mice (Kuma and Mizushima, 2008).

2.4. Breeding GFP-LC3 mice to other mouse models

The following will describe a general breeding strategy to produce GFP-LC3 in three different types of genetic mouse models: (1) transgene (e.g., with a disease-related mutation); (2) deletion of the gene of interest with conventional knockout; (3) deletion of the gene of interest with conditional knockout.

2.4.1. Transgenic (Tg) mice

$$\begin{array}{l} \text{Tg X/+} \times \text{GFP-LC3/+} \\ \downarrow \\ \text{Tg X/+; GFP-LC3/+} \\ \text{+/+; GFP-LC3/+} \\ \text{TgX/+; +/+} \\ \text{+/+; +/+} \end{array}$$

This is a simple breeding strategy that results in the generation of mice Tg X/+; GFP-LC3/+, which coexpress transgene X and the reporter GFP-LC3. Littermate +/+; GFP-LC3/+ can be used as a control for evaluating the specific effect of transgene X on GFP-LC3 distribution. This type of breeding was used in our previous study of autophagy in Lurcher mice (Wang *et al.*, 2006).

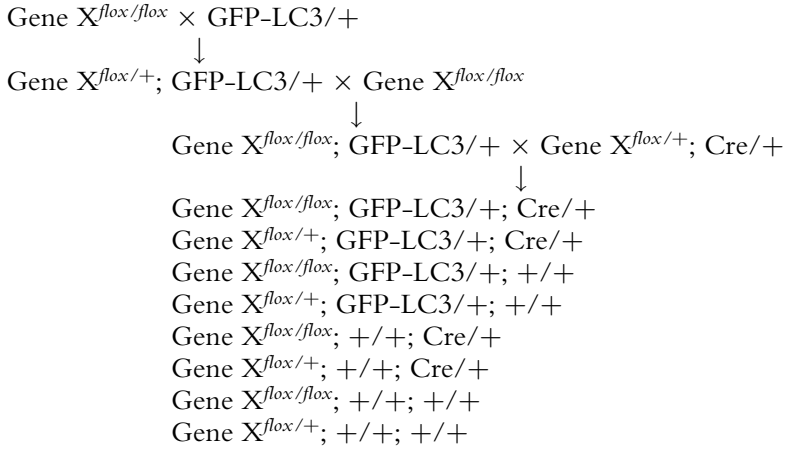
2.4.2. Conventional knockout mice

$$\begin{array}{l} \text{Gene X}^{+/-} \times \text{GFP-LC3/+} \\ \downarrow \\ \text{Gene X}^{+/-}; \text{GFP-LC3/+} \times \text{Gene X}^{+/-} \\ \downarrow \\ \begin{array}{l} \text{Gene X}^{-/-}; \text{GFP-LC3/+} \\ \text{Gene X}^{+/-}; \text{GFP-LC3/+} \\ \text{Gene X}^{+/+}; \text{GFP-LC3/+} \\ \text{Gene X}^{-/-}; +/+ \\ \text{Gene X}^{+/-}; +/+ \\ \text{Gene X}^{+/+}; +/+ \end{array} \end{array}$$

To express GFP-LC3 in mutant mice with gene X deletion, mouse breeding should be performed across two generations. The first breeding is responsible for generating Gene X^{+/-}; GFP-LC3/+ mice. The second breeding involves a back-cross of Gene X^{+/-}; GFP-LC3/+ to Gene X^{+/-}. This backcross generates mice Gene X^{-/-};GFP-LC3/+, which allows for the study of GFP-LC3 distribution in a gene X null background.

Littermate Gene $X^{+/-}$; GFP-LC3/+ or Gene $X^{+/+}$; GFP-LC3/+ is used as a control for the specific effect of gene X loss. This type of breeding was previously used in the study of autophagy in cathepsin D knockout mice (Koike *et al.*, 2005).

2.4.3. Conditional knockout mice



To express GFP-LC3 in mutant mice with a tissue/cell type-specific gene X deletion, the breeding will normally involve mice harboring a floxed gene X and mice expressing tissue/cell type-specific Cre, and the entire procedure will span over three generations. As shown in the above flow chart, the first two breedings will generate mice with homozygous floxed gene X and transgene GFP-LC3 (Gene $X^{flox/flox}$; GFP-LC3/+). In the third breeding, Gene $X^{flox/flox}$; GFP-LC3/+ mice will be crossed to Gene $X^{flox/+}$; Cre/+ mice to generate Gene $X^{flox/flox}$; GFP-LC3/+; Cre/+ mice in which GFP-LC3 is produced and gene X is deleted in the specific tissue/cell-type. We performed this type of breeding scheme to express GFP-LC3 in mutant mice with Purkinje cell-specific deletion of the autophagy gene *Atg7* ($Atg7^{flox/flox}$; *Pcp2-Cre/+*) (Komatsu *et al.*, 2007b).

3. ANALYSIS OF GFP-LC3 EXPRESSION AND SUBCELLULAR LOCALIZATION IN THE CNS

Perhaps all autophagy-related (ATG) genes including *Atg8/LC3* are expressed ubiquitously and their expression levels are highly regulated. However, since the expression of the transgenic GFP-LC3 is under the control of a nonspecific promoter (chicken β -actin promoter) (Mizushima *et al.*, 2004), GFP-LC3 levels may be artificially present in a given tissue/cell type and at a

certain time. Therefore, the application of GFP-LC3 transgenic mice is limited to the availability of the GFP-LC3 protein in certain tissues/cell types under study. A prior knowledge of GFP-LC3 expression in the tissue/cell type of interest in GFP-LC3 mice is helpful in designing experiments and interpreting data. The following describes the preparation of brain slices for the imaging of the GFP-LC3 puncta in CNS neurons. All protocols for handling mice should be approved by the appropriate institutional animal care and use committee or the equivalent committee in research institutes.

1. Anesthetize GFP-LC3 mice with ketamine at 100 mg/kg and xylazine at 10 mg/kg through the intraperitoneal (IP) route.
2. Perfuse the anesthetized mice transcardially with PBS (pH 7.4) followed by 4% paraformaldehyde in PBS using a peristaltic pump (Rainin).
3. Carefully remove the brain through dissection, and post fix the brain in 4% paraformaldehyde at 4 °C overnight.
4. Embed the freshly-fixed brain in 4%–5% low-melting-point agarose gel (Cambrex Bio Science Rockland, Rockland, ME, Cat. No. 50110).
5. After the gel block becomes solid, trim the agarose block containing the embedded brain into a cube with minimal size, properly orient and glue it on the stage with Krazy glue.
6. Section the brain tissue at 40–60 μm using a Vibratome (Tissue Sectioning and Bath Refrigeration Systems (Vibratome, St. Louis, MO)). Keep the slice in PBS at 4 °C.

(Optional: after step 3, the fixed brain can be cryoprotected by immersing the brain in 30% sucrose-PBS overnight. The complete penetration of sucrose is achieved when the brain tissue sinks to the bottom of a tube filled with 30% sucrose-PBS. Then the brain can be embedded in Tissue-Tek O. C.T. (Sakura Finetek, Cat. No. 4583) compound and sectioned through the use of a cryostat or sliding microtome on a frozen stage for thinner sections.)

7. For immunostaining, block the brain slices free floating with blocking buffer (PBS supplemented with 0.05% Triton X-100 and 10% goat serum (Invitrogen, Carlsbad, CA, Cat No. 16210-072) for 30 min and then incubate these slices with primary antibody (e.g., anti-GFP antibody) in blocking buffer at 4 °C overnight.
8. Wash the brain slices with PBS 3 times and then incubate these slices with the desired fluorophore-conjugated secondary antibody in blocking buffer in the dark for 45 min at room temperature.
9. Wash the brain slices with PBS 4 times (for the last time, keep the brain slices in PBS for 10 min in the dark).
10. Mount the slices with ProLong Gold antifade reagent (Invitrogen, Carlsbad, CA, Cat. No. P36930 or P36931 (with DAPI)) and 1.5-mm-thick coverslips.

(Optional: It is possible to image direct fluorescence of GFP-LC3 without the immunostaining procedure in certain areas of the CNS where GFP-LC3 levels are relatively high (e.g., cerebellar Purkinje cells, Fig. 8.1A,B); however, staining with anti-GFP antibody was shown to improve significantly the weak GFP-LC3 fluorescent signal in neurons presumably expressing low levels of GFP-LC3, Fig. 8.1C and 8.2).

11. Examine the fluorescent staining of these brain slices using a confocal laser-scanning microscope.

Notes:

1. Transgenic GFP-LC3 mice express high levels of GFP-LC3 in adult cerebellar Purkinje cells. As revealed by imaging direct fluorescence of

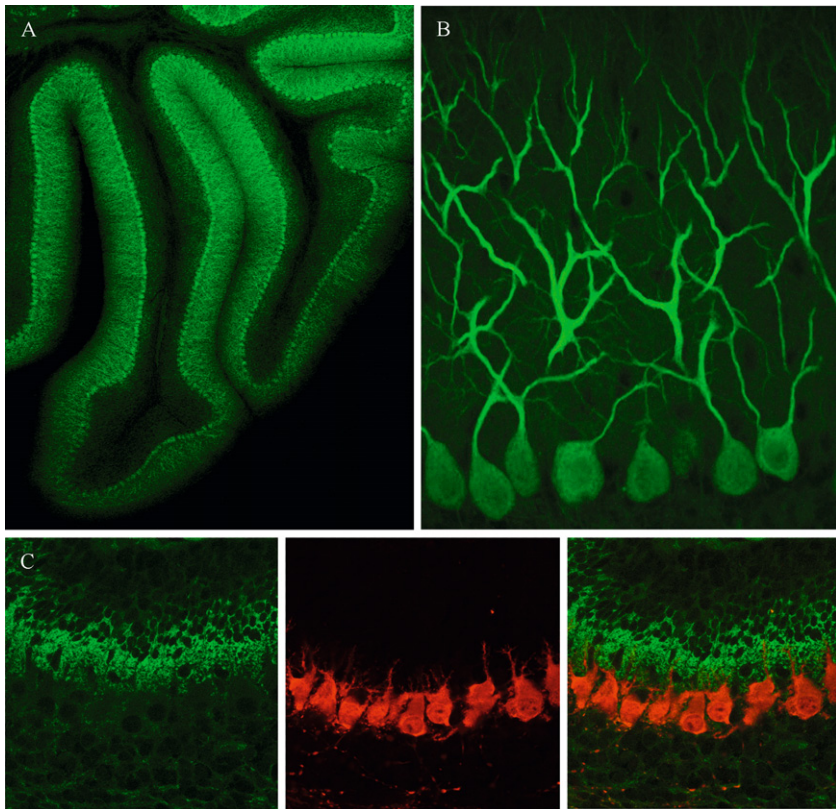


Figure 8.1 Expression of GFP-LC3 in the cerebellum of transgenic GFP-LC3 mice imaged with a confocal laser scanning microscope. (A) and (B) Direct imaging of fluorescence of GFP-LC3 produced in the Purkinje cell layer of an adult mouse at low (A) and high (B) magnifications, respectively. (C) Immunofluorescent staining of the P7 cerebellum with anti-GFP (green, left panel) and anti-calbindin (red, middle panel) antibodies. The merged image is shown in the right panel. GFP-LC3 expression is barely detected in Purkinje cells at P7, in contrast to adult cerebellum.

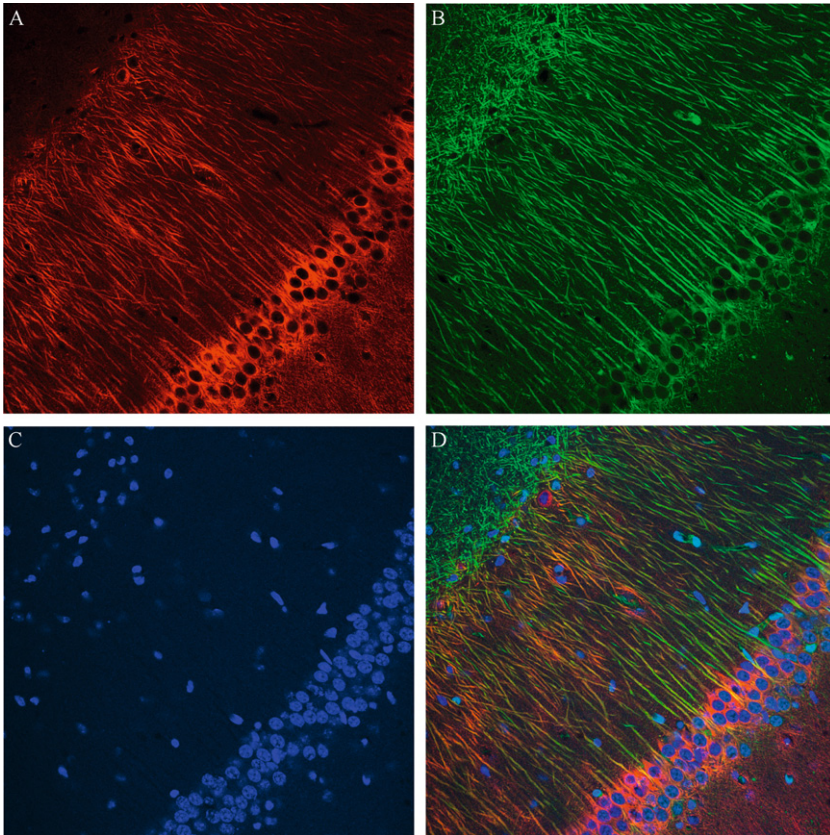


Figure 8.2 Expression of GFP-LC3 in hippocampal CA1 of transgenic GFP-LC3 mice imaged with a confocal laser scanning microscope. Hippocampal slices of GFP-LC3 transgenic mice were stained with anti-MAP2 antibody (A), anti-GFP antibody (B) and DAPI (for nuclei) (C). The merged image is shown in (D).

GFP-LC3 in the cerebellum, intense GFP-LC3 fluorescence is present in the entire Purkinje cell layer (Fig. 8.1A). Furthermore, GFP-LC3 is distributed in the Purkinje cell soma and primary dendrites in a largely diffuse pattern (Fig. 8.1B).

- Little GFP-LC3 is expressed in Purkinje cells of GFP-LC3 mice at early postnatal days (e.g., P7) (Fig. 8.1C). Cerebellar slices of GFP-LC3 mice at the age of P7 are stained with anti-GFP antibody (affinity purified polyclonal rabbit IgG generated in house (Cristea *et al.*, 2005)) and anti-calbindin antibody (for labeling Purkinje cells in cerebella, monoclonal mouse IgG D-28K, 1:1000; Swant, Bellinzona, Switzerland, Cat. No. 300), followed by labeling with Alexa Fluor 488 goat antirabbit IgG and Alexa Fluor 594 goat antimouse IgG secondary antibodies (1:500, Invitrogen, Carlsbad, CA, Cat. Nos. A11034 and A11032, respectively).

In contrast to adult Purkinje cells, P7 Purkinje cells (in red) express very little GFP-LC3 (in green), whereas cerebellar granule neurons express high levels of GFP-LC3 in the background (Fig. 8.1C).

3. Although imaging direct fluorescence of GFP-LC3 shows that adult hippocampal neurons (CA1) express weak levels of GFP-LC3 (data not shown), staining with anti-GFP antibody and Alexa 488-conjugated secondary antibody yields enhanced GFP-LC3 fluorescence in CA1 neuron at soma and dendrites (Fig. 8.2). The slices are counter-stained with anti-MAP2 antibody (for detection of dendrites), followed by Alexa-594 conjugated secondary antibody (in red). Nuclei of neurons are labeled with DAPI (in blue).

4. ANALYSIS OF P62/SQSTM1 AND UBIQUITINATED PROTEIN INCLUSIONS IN THE CNS

Targeted deletion of essential autophagy genes in mouse brain provides an opportunity to understand the physiological function of autophagy in the CNS (Hara *et al.*, 2006; Komatsu *et al.*, 2006). In these autophagy-deficient brains, levels of ubiquitinated proteins are markedly increased and a large number of ubiquitinated protein inclusions are formed inside neurons. In parallel, p62/SQSTM1 levels are significantly enhanced and p62/SQSTM1 is accumulated in protein inclusion bodies (Komatsu *et al.*, 2007a). Therefore, increased levels of ubiquitinated proteins and p62/SQSTM1 are important traits of autophagy deficiency in CNS neurons. Assaying p62/SQSTM1 protein levels has increasingly been recognized as a readout for autophagy activity since first demonstrated in our study (Wang *et al.*, 2006).

4.1. Immunohistochemistry staining of p62/SQSTM1

1. Block the brain slices free floating with blocking buffer (PBS supplemented with 0.05% Triton X-100 and 10% goat serum) for 30 min and then incubate slides with guinea pig anti-p62 (1:500, American Research Products, Belmont, MA, Cat. No. 03-GP62-C) in blocking buffer at 4 °C overnight.
2. Wash the brain slices with PBS 3 times and then incubate with Alexa Fluor 488 goat anti-guinea pig secondary antibody (1:1000, Invitrogen, Carlsbad, CA, Cat No. A11073) in blocking buffer in the dark at room temperature for 45 min.
3. Wash the brain slices with PBS 4 times (for the last time, keep the brain slices in PBS for 10 min in the dark).

4. Mount the slice on glass slides with ProLong Gold antifade reagent and 1.5-mm-thick coverslips.
5. Examine the fluorescent staining of these brain slices using a confocal laser-scanning microscope.

Notes:

Immunofluorescent staining of p62 in brain tissues has assisted us in assessing the change in autophagic activity in *Lurcher* Purkinje cells. Previously, we showed that, in both *Lurcher* and *Atg7^{lox/lox}; Pcp2-Cre* mice, axon terminals of Purkinje cell undergo dystrophic swelling and degeneration (Komatsu *et al.*, 2007; Wang *et al.*, 2006). As expected, *Atg7* deletion-mediated autophagy deficiency causes an increase in p62 protein levels at swollen axon terminals of *Atg7^{lox/lox}; Pcp2-Cre* Purkinje cells, whereas little change in p62 protein levels is seen at axon terminals of *Lurcher* Purkinje cells (Fig. 8.3). This result suggests that autophagy is induced rather than blocked in axon terminals of *Lurcher* Purkinje cells (Wang *et al.*, 2006).

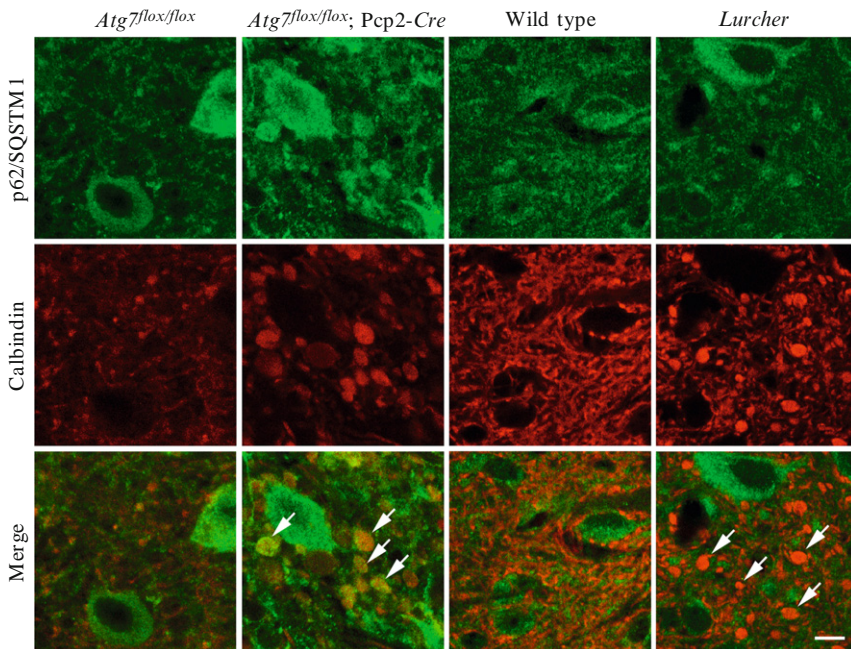


Figure 8.3 Immunostaining of p62/SQSTM1 in dystrophic swellings of Purkinje cell axon terminals. Cerebellar slices at deep cerebellar nuclei from *Atg7^{lox/lox}; Pcp2-Cre* mice and *Lurcher* mice were stained with anti-p62/SQSTM1 (in green) and anti-calbindin (in red) antibodies. The p62/SQSTM1 is accumulated in the dystrophic swellings of axon terminals (white arrows) from *Atg7^{lox/lox}; Pcp2-Cre* Purkinje cells but not *Lurcher* Purkinje cells. Scale bar: 10 μ m. This figure is modified from (Komatsu *et al.*, 2007b) with permission.

5. TRANSMISSION ELECTRON MICROSCOPY (TEM) ANALYSIS OF AUTOPHAGOSOMES

5.1. Tissue fixation and processing for ultrastructural studies

1. Perfuse the anesthetized mouse transcardially with 100 mL of room-temperature 1% formaldehyde/2% glutaraldehyde fixative in 0.1 M PBS, pH 7.4, after flushing the vasculature with warm (37 °C) heparinized (2 U/mL; American Pharmaceutical Partners, Cat. No. 401586A) 0.01M PBS, pH 7.4. The formaldehyde solution should be prepared from EM grade purified paraformaldehyde powder (Electron Microscopy Sciences, Cat. No. 19210). The glutaraldehyde should be specified as EM Grade Distillation Purified and obtained from a reliable source for EM products such as Electron Microscopy Sciences (www.emsdiasum.com), Ernest Fullam (www.fullam.com), or Ted Pella (www.tedpella.com). Although the formaldehyde solution may be prepared several days in advance, the glutaraldehyde should not be added to the fixative solution until shortly before use.
2. After the fixative has been delivered, leave the mouse in place for approximately 60 min.
3. Harvest the brain and immediately immerse it in a vial of cold (4 °C) perfusion fixative. Leave overnight at 4 °C.
4. Cut 50- to 100- μ m-thick Vibratome sections through the region(s) of interest, keeping the tissue block and sections cold by using the Tissue Sectioning and Bath Refrigeration System, or by placing 4–5 cubes of frozen 0.1 M phosphate buffer, pH 7.4 (PB), in the Vibratome well filled with cold PB. Place the sections in wells of a 24-well plastic plate containing PB, on ice.
5. Further dissect the sections in a large Petri dish of PB so that the sections contain only the region(s) of interest. The sections should be no larger than 5 mm on a side. Place the dissected sections in glass vials containing PB, fitted with screw caps having aluminum (not paper) inner linings, on ice. Sections from the same region/animal/condition may be pooled in a single vial.

Note: All subsequent steps should be performed in a fume hood, with protective eyewear and gloves.

6. Once all the sections are dissected, rinse them twice in ice-cold PB, and then osmicate (1% OsO₄ in PB with 7% dextrose) for 1 h in the covered glass vials, on ice.
7. Dehydrate the specimens in ascending concentrations of ice-cold ethanol diluted in distilled water, on ice, as follows:
 - 1 rinse in 50% ethanol, 10 min

- 1 rinse in 70% ethanol, 10 min
- 2 rinses in 95% ethanol, 10 min each
- 2 rinses in 100% ethanol, 10 min each
- 2 rinses in propylene oxide, 10 min each
8. Infiltrate the specimens with resin by immersing them for 30 min in a 1:1 mixture of epoxy resin (Epon, Araldite or Epon-Araldite; Electron Microscopy Sciences Cat. Nos. RT 14120, RT 13920 and RT 13940, respectively) and propylene oxide (Electron Microscopy Sciences, Cat. No. 20410). Replace the solution with 100% resin, and leave overnight on a vertical rotator at 4 °C.
9. Embed the sections in capsules, molds or between Aclar sheets (Electron Microscopy Sciences, Cat. Nos. 70000-B, 70905-01 and 50425-10, respectively) or plastic coverslips (Fisher Scientific, Cat. No. 12-547). Cure in an oven at 60 °C for 3 days.
10. Trim the embedded tissue to contain the area of interest and then thin-section using an ultramicrotome onto mesh or Formvar-coated slot grids (Electron Microscopy Sciences, Cat. Nos. 0200-CU, RT-15830 and G7530-Cu, respectively).
11. Sections can be contrasted using 5% aqueous uranyl acetate (15–30 min) and 0.15% lead acetate or citrate (10 to 30 min). Alternatively, the sections can be stained with uranyl deposits during the dehydration step (step 7 above) using uranyl acetate diluted in 70% ethanol. Insert this step between two 70% ethanol rinses, prior to the 95% ethanol rinse. (One resource for general information about TEM tissue processing is the Practical Methods in Electron Microscopy series (Elsevier) edited by A. M. Glauert. See also the chapter by Ylä-Anttila *et al.*, in this volume.)

5.2. Tissue fixation and processing for pre-embedding immuno-electron microscopy

1. Perfuse the anesthetized mouse transcardially with 100 mL of room temperature 4% formaldehyde/0.25% glutaraldehyde fixative in 0.1 M PBS, pH 7.4, after flushing the vasculature with warm (37 °C) heparinized (2 U/mL) 0.01 M PBS, pH 7.4. Prepare the fixative as described above.
2. Harvest the brain, block the region(s) of interest, and immerse the block in a beaker containing cold (4 °C) glutaraldehyde-free fixative. Leave for 90 min at 4 °C.
3. Place the blocks in a series of ascending concentrations of sucrose (7%, 10%, 20%) diluted in PB, 30 min each, and leave overnight at 4 °C in fresh 20% sucrose in PB.
4. In a fume hood, place a wide-mouthed beaker containing isopentane within a larger basin of acetone cooled with dry ice. Transfer the tissue

block to a small (e.g., 10 mL) Pyrex beaker, and add just enough fresh 20% sucrose to cover the block. Place the 10 mL beaker in the bath using forceps, and leave until the sucrose appears frozen. Gently remove the beaker using forceps, and allow it to thaw completely at room temperature, undisturbed. Repeat this procedure once. This process aids antibody penetration.

5. Cut 50- to 100- μm -thick Vibratome sections as described previously (*Tissue fixation and processing for ultrastructural studies*, Step 4).
6. Process the sections for peroxidase immunocytochemistry. After quenching endogenous peroxidase by immersing the sections in 0.3% H_2O_2 for 30 min at room temperature (RT), rinse the sections thoroughly with PBS (6 rinses, 10 min each) and then place them in blocking buffer (5% normal serum of the donor species of the secondary antibody in PBS) overnight at 4 °C. Bring the sections to RT, add primary antisera or control sera, and then incubate overnight at 4 °C. Sections are then rinsed thoroughly with PBS (6 rinses, 10 min each) incubated with biotinylated secondary antibodies for 2–3 hrs at RT, rinsed again, and then incubated with streptavidin-HRP (Zymed Laboratories, San Francisco, CA) for 1 h at RT.
7. To visualize peroxidase conjugates, incubate the sections in 0.05% diaminobenzidine (DAB; Sigma Cat No. D4293) with 0.01% H_2O_2 in 0.1 M Tris buffer, pH 7.6 (TB; 3.31g Tris-HCl and 0.49 g Tris Base in 500 ml distilled water) for 5–10 min at RT. After the tissue has been incubated in DAB, rinse once with TB, twice with PB, and then process for electron microscopy as described in *Tissue fixation and processing for ultrastructural studies*, starting at step 5. The DAB reaction product is visible by TEM as an electron-dense reaction product, and is readily discernable from the punctate gold particles of varying size used for postembedding labeling.

5.3. Tissue fixation and processing for post-embedding immunogold TEM localization

1. Follow Steps 1 and 2 of the procedure “Tissue fixation and processing for preembedding immuno-electron microscopy.”
2. Cut 100- μm to 1-mm thick Vibratome sections through the region(s) of interest, keeping the tissue block and sections cold by using the Tissue Sectioning and Bath Refrigeration System, or by placing 4–5 cubes of frozen 0.1 M PB in the Vibratome well filled with cold PB. Place the sections in wells containing PB, on ice.
3. Further dissect the sections in a large Petri dish of PB so the sections contain only the region(s) of interest. The sections should be no larger than 2 mm on a side. Place the dissected sections in glass or plastic vials containing PB, fitted with screw caps.

4. Cryoprotect the tissue at room temperature using increasing concentrations of glycerol in PB (10%, 20%, 30%, 1 h each), then store overnight in 30% glycerol at 4 °C.
5. Freeze-plunging and subsequent tissue embedment require specialized equipment, available from multiple vendors including the electron microscopy sources identified previously. Examples are the Reichert KF 80 and the Leica EM FSP freeze-plunger units and the Leica AFS embedding unit (Leica Microsystems). The sections are glued to aluminum flat-headed pins and then plunge-frozen using the appropriate equipment. The sections are then resin-embedded and UV-polymerized using the automatic reagent dilution and handling systems of the embedment units. In most processing/embedding units, 20–24 specimens can be processed in one run.
6. Trim the embedded tissue to contain the region(s) of interest and then thin-section using an ultramicrotome and transfer onto nickel or gold mesh or Formvar-coated slot grids (Electron Microscopy Sciences, Cat. Nos. G100-Ni, G200-Au, G2010-Ni, and GG205-Ni). Mount the grids in Hiraoka support plates (Electron Microscopy Sciences, Cat. No. 71560-10).
7. The grids are rinsed with TB-saline (4.5 g NaCl in 500 ml TB) containing 0.1% Triton X-100 (TBST), and then with 0.1% NaBH₄, 50 mM glycine in TBST, blocked in 10% normal serum (NS) in TBST, incubated in primary antibody (e.g., anti-GFP antibody) diluted in 1% NS in TBST (2 h at room temperature), rinsed and blocked again, then incubated for 1 h at room temperature with gold-conjugated secondary antibodies (Electron Microscopy Sciences) diluted 1:20 in 1% NS in TBST with 0.5% polyethylene glycol, and rinsed again. For double labeling using gold particles of different sizes, expose the grids to paraformaldehyde vapors for 1 h, then rinse thoroughly and repeat the labeling procedure beginning with incubation in the primary antibody if the double labeling has both primary antibodies made in the same donor species. At the conclusion of all labeling, contrast the sections with 1% aqueous uranyl acetate (15–30 min) and 0.3% lead citrate diluted in water (10–30 min). Visualization of smaller (1–10 nm) gold particles is often aided by use of silver enhancement (Electron Microscopy Sciences Cat. No. 25521). This process assists localization of the gold particles, but sacrifices the punctate signal provided by nonenhanced gold particles.

5.4. TEM identification of double-membraned vacuoles

Autophagosomes are recognizable in the cytoplasm of neurons as double-membrane bound vacuoles, with cross-sectional diameters of approximately 0.1–0.5 μm . Our studies suggest that autophagosomes may be

synthesized locally in axon terminals and may undergo axonal transport to the soma where lysosomes are normally present for final degradation (Komatsu *et al.*, 2007b). Many of the double-membraned vacuoles found in axon terminals appear to be derived from the invagination of neighboring oligodendrocytes, a process which is poorly understood but may be related to endocytosis via the axolemma and cytoplasmic membranes of oligodendrocytes (Eddleman *et al.*, 1998; Zhang *et al.*, 2005). Additionally, we have observed the formation of double-membraned vacuoles that do not appear to be derived from the invasion of oligodendrocytes (Komatsu *et al.*, 2007b). Speculatively, as previously reported, the vacuoles may originate from axonal subsurface cisternae (Li *et al.*, 2005) or smooth ER (Broadwell and Cataldo, 1984).

5.5. Quantification of double-membraned vacuoles

Quantification of double-membraned vacuoles in TEM material can be accomplished using a point-counting method. Construct a grid using Photoshop (or similar software used to analyze the TEM images). Overlay each TEM image with the grid image. Count the number of vacuoles (for profile identification, see *TEM identification of double-membraned vacuoles* section) overlaid by at least one cross-point of the grid and the total number of cross points within the vacuoles (Fig. 8.4). Calculate the total area of each micrograph to determine the density of autophagosomes per unit area. Counting should be performed double-blind, and equal areas of tissue should be analyzed for all conditions. Volumetric densities can be obtained by factoring in the section thickness.

6. CONCLUSION

Recent studies have begun to explore the potential of autophagy as a drug target in treating neurodegenerative disease. Thus, delineating the neuronal autophagy process and the mechanism by which autophagy is involved in various pathological conditions will be crucial for a better understanding of neurodegeneration and the design of therapeutic drugs. Although GFP-LC3 transgenic mice have been successfully used as a reporter to study autophagic activity in the CNS, limitations in their application as an autophagy reporter have also been recognized. It is of particular importance to dissect the basal level of autophagic activity in healthy neurons where GFP-LC3 may serve as a poor marker. Recent studies indicate that p62/SQSTM1, a selective substrate of autophagy, can also be used as an autophagic marker for neuronal autophagic activity.

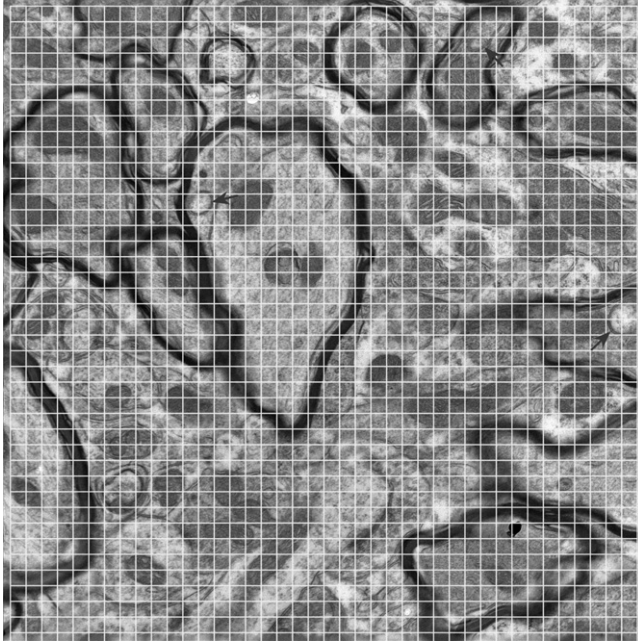


Figure 8.4 An example of using the point-counting method to quantify double-membraned vacuole-like structures in the deep cerebellar nuclei of *Atg7^{flox/flox}; Pcp2-Cre* cerebellum. The electron micrograph (with an area of $50 \mu\text{m}^2$) is overlaid with a Photoshop-generated grid (41×41). The mesh size of the grid is chosen depending on the frequency and size of the structures. In this example, the number of these structures containing at least one intersection of the grid was determined to be 3 (arrows). The volume of the structures was counted as the number of intersections within the structures and was determined in this example to be 8.

With our growing knowledge of the neuronal autophagy process, we anticipate identifying ever more specific autophagy markers to assist in assaying autophagic activity in the CNS.

ACKNOWLEDGMENTS

This study was supported by the NIH to Z.Y (NS060123-02), GRH (DC008846-01) and B.T.C (RR00862 and RR022220).

REFERENCES

- Anglade, P., Vyas, S., Javoy-Agid, F., Herrero, M. T., Michel, P. P., Marquez, J., Mouatt-Prigent, A., Ruberg, M., Hirsch, E. C., and Agid, Y. (1997). Apoptosis and autophagy in nigral neurons of patients with Parkinson's disease. *Histol. Histopathol.* **12**, 25–31.

- Bjørkøy, G., Lamark, T., Brech, A., Outzen, H., Perander, M., Overvatn, A., Stenmark, H., and Johansen, T. (2005). p62/SQSTM1 forms protein aggregates degraded by autophagy and has a protective effect on huntingtin-induced cell death. *J. Cell Biol.* **171**, 603–614.
- Broadwell, R. D., and Cataldo, A. M. (1984). The neuronal endoplasmic reticulum: Its cytochemistry and contribution to the endomembrane system. II. Axons and terminals. *J. Comp. Neurol.* **230**, 231–248.
- Cao, Y., Espinola, J. A., Fossale, E., Massey, A. C., Cuervo, A. M., MacDonald, M. E., and Cotman, S. L. (2006). Autophagy is disrupted in a knock-in mouse model of juvenile neuronal ceroid lipofuscinosis. *J. Biol. Chem.* **281**, 20483–20493.
- Cataldo, A. M., Hamilton, D. J., Barnett, J. L., Paskevich, P. A., and Nixon, R. A. (1996). Properties of the endosomal-lysosomal system in the human central nervous system: Disturbances mark most neurons in populations at risk to degenerate in Alzheimer's disease. *J. Neurosci.* **16**, 186–199.
- Cristea, I. M., Williams, R., Chait, B. T., and Rout, M. P. (2005). Fluorescent proteins as proteomic probes. *Mol. Cell. Proteomics* **4**, 1933–1941.
- Chu, C. T. (2006). Autophagic stress in neuronal injury and disease. *J. Neuropathol. Exp. Neurol.* **65**, 423–432.
- Dixon, J. S. (1967). "Phagocytic" lysosomes in chromatolytic neurones. *Nature* **215**, 657–658.
- Eddleman, C. S., Ballinger, M. L., Smyers, M. E., Fishman, H. M., and Bittner, G. D. (1998). Endocytotic formation of vesicles and other membranous structures induced by Ca^{2+} and axolemmal injury. *J. Neurosci.* **18**, 4029–4041.
- Filimonenko, M., Stuffers, S., Raiborg, C., Yamamoto, A., Malerod, L., Fisher, E. M., Isaacs, A., Brech, A., Stenmark, H., and Simonsen, A. (2007). Functional multivesicular bodies are required for autophagic clearance of protein aggregates associated with neurodegenerative disease. *J. Cell Biol.* **179**, 485–500.
- Hara, T., Nakamura, K., Matsui, M., Yamamoto, A., Nakahara, Y., Suzuki-Migishima, R., Yokoyama, M., Mishima, K., Saito, I., Okano, H., and Mizushima, N. (2006). Suppression of basal autophagy in neural cells causes neurodegenerative disease in mice. *Nature* **441**, 885–889.
- Ko, D. C., Milenkovic, L., Beier, S. M., Manuel, H., Buchanan, J., and Scott, M. P. (2005). Cell-autonomous death of cerebellar purkinje neurons with autophagy in Niemann-Pick type C disease. *PLoS Genet.* **1**, 81–95.
- Koike, M., Shibata, M., Tadakoshi, M., Gotoh, K., Komatsu, M., Waguri, S., Kawahara, N., Kuida, K., Nagata, S., Kominami, E., Tanaka, K., and Uchiyama, Y. (2008). Inhibition of autophagy prevents hippocampal pyramidal neuron death after hypoxic-ischemic injury. *Am. J. Pathol.* **172**, 454–469.
- Koike, M., Shibata, M., Waguri, S., Yoshimura, K., Tanida, I., Kominami, E., Gotow, T., Peters, C., von Figura, K., Mizushima, N., Saftig, P., and Uchiyama, Y. (2005). Participation of autophagy in storage of lysosomes in neurons from mouse models of neuronal ceroid-lipofuscinoses (Batten disease). *Am. J. Pathol.* **167**, 1713–1728.
- Komatsu, M., Waguri, S., Chiba, T., Murata, S., Iwata, J., Tanida, I., Ueno, T., Koike, M., Uchiyama, Y., Kominami, E., and Tanaka, K. (2006). Loss of autophagy in the central nervous system causes neurodegeneration in mice. *Nature* **441**, 880–884.
- Komatsu, M., Waguri, S., Koike, M., Sou, Y. S., Ueno, T., Hara, T., Mizushima, N., Iwata, J., Ezaki, J., Murata, S., Hamazaki, J., Nishito, Y., et al. (2007a). Homeostatic levels of p62 control cytoplasmic inclusion body formation in autophagy-deficient mice. *Cell* **131**, 1149–1163.
- Komatsu, M., Wang, Q. J., Holstein, G. R., Friedrich, V. L. Jr., Iwata, J., Kominami, E., Chait, B. T., Tanaka, K., and Yue, Z. (2007b). Essential role for autophagy protein Atg7 in the maintenance of axonal homeostasis and the prevention of axonal degeneration. *Proc. Natl. Acad. Sci. USA* **104**, 14489–14494.

- Kuma, A., and Mizushima, N. (2008). Chromosomal mapping of the GFP-LC3 transgene in GFP-LC3 mice. *Autophagy* **4**, 61–62.
- Lee, J. A., Beigneux, A., Ahmad, S. T., Young, S. G., and Gao, F. B. (2007). ESCRT-III dysfunction causes autophagosome accumulation and neurodegeneration. *Curr. Biol.* **17**, 1561–1567.
- Li, Y. C., Li, Y. N., Cheng, C. X., Sakamoto, H., Kawate, T., Shimada, O., and Atsumi, S. (2005). Subsurface cisterna-lined axonal invaginations and double-walled vesicles at the axonal-myelin sheath interface. *Neurosci. Res.* **53**, 298–303.
- Martinez-Vicente, M., Sovak, G., and Cuervo, A. M. (2005). Protein degradation and aging. *Exp. Gerontol.* **40**, 628–633.
- Matthews, M. R., and Raisman, G. (1972). A light and electron microscopic study of the cellular response to axonal injury in the superior cervical ganglion of the rat. *Proc. R. Soc. Lond. B. Biol. Sci.* **181**, 43–79.
- Mizushima, N., Yamamoto, A., Matsui, M., Yoshimori, T., and Ohsumi, Y. (2004). *In vivo* analysis of autophagy in response to nutrient starvation using transgenic mice expressing a fluorescent autophagosome marker. *Mol. Biol. Cell* **15**, 1101–1111.
- Nixon, R. A. (2006). Autophagy in neurodegenerative disease: Friend, foe or turncoat? *Trends Neurosci.* **29**, 528–535.
- Nixon, R. A., Wegiel, J., Kumar, A., Yu, W. H., Peterhoff, C., Cataldo, A., and Cuervo, A. M. (2005). Extensive involvement of autophagy in Alzheimer disease: An immuno-electron microscopy study. *J. Neuropathol. Exp. Neurol.* **64**, 113–122.
- Pacheco, C. D., Kunkel, R., and Lieberman, A. P. (2007). Autophagy in Niemann-Pick C disease is dependent upon Beclin-1 and responsive to lipid trafficking defects. *Hum. Mol. Genet.* **16**, 1495–1503.
- Roizin, L., Stellar, S., Willson, N., Whittier, J., and Liu, J. C. (1974). Electron microscope and enzyme studies in cerebral biopsies of Huntington's chorea. *Trans. Am. Neurol. Assoc.* **99**, 240–243.
- Rubinsztein, D. C., DiFiglia, M., Heintz, N., Nixon, R. A., Qin, Z.-H., Ravikumar, B., Stefanis, L., and Tolkovsky, A. (2005). Autophagy and its possible roles in nervous system diseases, damage and repair. *Autophagy* **1**, 11–22.
- Settembre, C., Fraldi, A., Jahreiss, L., Spampinato, C., Venturi, C., Medina, D., de Pablo, R., Tacchetti, C., Rubinsztein, D. C., and Ballabio, A. (2008). A block of autophagy in lysosomal storage disorders. *Hum. Mol. Genet.* **17**, 119–129.
- Sikorska, B., Liberski, P. P., Giraud, P., Kopp, N., and Brown, P. (2004). Autophagy is a part of ultrastructural synaptic pathology in Creutzfeldt-Jakob disease: A brain biopsy study. *Int. J. Biochem. Cell Biol.* **36**, 2563–2573.
- Wang, Q. J., Ding, Y., Kohtz, S., Mizushima, N., Cristea, I. M., Rout, M. P., Chait, B. T., Zhong, Y., Heintz, N., and Yue, Z. (2006). Induction of autophagy in axonal dystrophy and degeneration. *J. Neurosci.* **26**, 8057–8068.
- Yue, Z. (2007). Regulation of neuronal autophagy in axon: Implication of autophagy in axonal function and dysfunction/degeneration. *Autophagy* **3**, 139–141.
- Zhang, P., Land, W., Lee, S., Juliani, J., Lefman, J., Smith, S. R., Germain, D., Kessel, M., Leapman, R., Rouault, T. A., and Subramaniam, S. (2005). Electron tomography of degenerating neurons in mice with abnormal regulation of iron metabolism. *J. Struct. Biol.* **150**, 144–153.